The Astrophysical Journal, 712:274–286, 2010 March 20 doi:10.1088/0004-637X/712/1/274

SPITZER SPECTROSCOPY OF THE TRANSITION OBJECT TW Hya

Joan R. Najita[1], John S. Carr[2], Stephen E. Strom[1], Dan M. Watson[3], Ilaria Pascucci[4], David Hollenbach[5], Uma Gorti[5,6], and Luke Keller[7]
[1] National Optical Astronomy Observatory, 950 N. Cherry Ave., Tucson, AZ 85719, USA
[2] Naval Research Laboratory, Code 7211, Washington, DC 20375, USA
[3] University of Rochester, Department of Physics and Astronomy, University of Rochester, Rochester, NY 14627, USA
[4] Space Telescope Science Institute, 3700 San Martin Drive, Baltimore, MD 21218, USA
[5] SETI Institute, 515 North Whisman Road, Mountain View, CA 94043, USA
[6] NASA Ames Research Center, Moffett Field, CA 94035, USA
[7] Department of Physics, Ithaca College, Ithaca, NY 14850, USA
Received 2009 November 16; accepted 2010 February 3; published 2010 February 26

ABSTRACT

We report sensitive *Spitzer* IRS spectroscopy in the 10–20 μm region of TW Hya, a nearby T Tauri star. The unusual spectral energy distribution of the source, that of a "transition object," indicates that the circumstellar disk in the system has experienced significant evolution, possibly as a result of planet formation. The spectrum we measure is strikingly different from that of other classical T Tauri stars reported in the literature, displaying no strong emission features of H_2O, C_2H_2, or HCN. The difference suggests that the inner planet formation region ($\lesssim$5 AU) of the gaseous disk has evolved physically and/or chemically away from the classical T Tauri norm. Nevertheless, TW Hya does show a rich spectrum of emission features of atoms (H I, [Ne II], and [Ne III]) and molecules (H_2, OH, CO_2, HCO^+, and possibly CH_3), some of which are also detected in classical T Tauri spectra. The properties of the neon emission are consistent with an origin for the emission in a disk irradiated by X-rays (with a possible role for additional irradiation by stellar EUV). The OH emission we detect, which also likely originates in the disk, is hot, arising from energy levels up to 23,000 K above ground, and may be produced by the UV photodissociation of water. The H I emission is surprisingly strong, with relative strengths that are consistent with case B recombination. While the absence of strong molecular emission in the 10–20 μm region may indicate that the inner region of the gaseous disk has been partly cleared by an orbiting giant planet, chemical and/or excitation effects may be responsible instead. We discuss these issues and how our results bear on our understanding of the evolutionary state of the TW Hya disk.

Key words: circumstellar matter – planetary systems – protoplanetary disks – stars: individual (TW Hya) – stars: pre-main sequence

Online-only material: color figures

1. INTRODUCTION

Spectroscopy with the *Spitzer Space Telescope* has opened a new window on the gas in the planet formation region of circumstellar disks (<5 AU). It has revealed the presence of organic molecules in this inner region of the disk (Lahuis et al. 2006b; Carr & Najita 2008) and shown that water emission from disks is both more commonly occurring and extends to larger radii than previously known from ground-based observations (Carr & Najita 2008; Salyk et al. 2008). *Spitzer* spectroscopy has also demonstrated that [Ne II], which was predicted to arise from irradiated disk atmospheres (Glassgold et al. 2007), is commonly present in spectra of T Tauri stars (Pascucci et al. 2007; Lahuis et al. 2007; Espaillat et al. 2007; Guedel et al. 2009). These diagnostics offer the opportunity to study the evolution of gaseous disks and to obtain new insights into the processes by which disks evolve.

Transition objects are an interesting class of sources to study in this context. Their spectral energy distributions (SEDs) are interpreted as arising from an optically thin inner disk (within an opacity "hole" of radius $R_{\rm hole}$) that is surrounded by an optically thick outer disk (beyond $R_{\rm hole}$). Such an SED can arise in several ways, as a consequence of grain growth (e.g., Strom et al. 1989; Dullemond & Dominik 2005), giant planet formation (e.g., Skrutskie et al. 1990; Marsh & Mahoney 1992; Lubow et al. 1999; Bryden et al. 1999), or disk photoevaporation (Clarke et al. 2001; Alexander et al. 2006). Transition objects might arise in any of these ways, and the evolutionary path for any given T Tauri star, which may or may not involve a stint as a transition object, may depend on initial conditions such as the initial disk mass.

The above processes do make different predictions for the stellar accretion rates and disk masses under which a transitional SED will arise (Najita et al. 2007b; Alexander & Armitage 2007). As a result, stellar accretion rates and disk masses have been employed previously in diagnosing the nature of transition objects (Najita et al. 2007b; Cieza et al. 2008; Alexander & Armitage 2009).

Because these processes also make different predictions for the structure of the gaseous disk, studying the gaseous disks of transition objects is potentially another tool that can be used to distinguish among these possibilities (Najita et al. 2007b, 2008). This approach, the one taken here, may therefore offer insights into how planets form and disks dissipate.

At a distance of 51 pc (Mamajek 2005), TW Hya is the nearest T Tauri star and a well-known transition object. Its SED indicates that the region of the disk within $R_{\rm hole} \sim 4$ AU of the star is optically thin in the continuum (Calvet et al. 2002; Uchida et al. 2004). Higher angular resolution interferometric results at 7 mm (Hughes et al. 2007) and at 10 μm (Ratzka et al.

Table 1
Observing Log for TW Hya SH Data Sets

Data Set	Date	AOR	Ramp (s)	On-Source (s)	Off-Source (s)
GTO	2004 Jan 4	3571456	6	12	0
SH1	2006 Jul 1	18017792[a]	30	120	120
SH2	2008 Jan 7	24402944	30	600	300

Note. [a] AOR for sky observations: 18018048, 18018304.

2007) further confirm a deficit of continuum emission from the central region of the disk. TW Hya is also an unusual T Tauri star in other respects. Despite its advanced age (∼10 Myr), it has a massive disk (Wilner et al. 2000; Calvet et al. 2002) and is still accreting (Muzerolle et al. 2000; Johns-Krull et al. 2000; Herczeg et al. 2004; Alencar & Batalha 2002). TW Hya is also a source of energetic UV emission (Herczeg et al. 2004; Bergin et al. 2004) and emits strongly in X-rays (Kastner et al. 1999; Stelzer & Schmitt 2004; Robrade & Schmitt 2006).

Spectroscopy of TW Hya taken with the *Spitzer* Infrared Spectrograph (IRS) has been reported previously, with an emphasis on the shape of the mid-infrared continuum and what it says about the radial distribution of the dust opacity in the disk (Uchida et al. 2004). Based on a reanalysis of the same data, Ratzka et al. (2007) reported the detection of emission lines of H I 6–5, H I 7–6, and [Ne II]. The [Ne II] emission from TW Hya has been studied from the ground at high spectral resolution by Herczeg et al. (2007) and Pascucci & Sterzik (2009).

Here, we report further IRS spectroscopy of TW Hya obtained at higher signal to noise in two later epochs. The spectra show a rich suite of emission features, both atomic and molecular, some of which have been detected before in spectra of classical T Tauri stars. We discuss the physical processes that may be responsible for the emission (Section 3). The spectra are also strikingly different from the spectra of classical T Tauri stars, in that they lack strong emission features of H_2O, C_2H_2, and HCN. This suggests that the inner gaseous disk has evolved physically and/or chemically away from the classical T Tauri norm. We discuss how these differences bear on our understanding of the evolutionary state of the disk (Section 4.1). We also discuss where in the system the detected emission features may arise (Section 4.2).

2. OBSERVATIONS AND DATA REDUCTION

TW Hya was observed twice with the short-high (SH) module of the IRS (Houck et al. 2004) on board the *Spitzer Space Telescope* (Werner et al. 2004) as part of the program GO 30300. A first epoch spectrum (hereinafter SH1) was acquired in 2006. A second, longer integration spectrum (hereinafter SH2) was acquired in 2008. An earlier, shorter integration spectrum that pre-dates both of the spectra from our GO program was acquired in 2004 as part of the IRS GTO program (hereinafter GTO). The GTO data have been presented previously by Uchida et al. (2004) and Ratzka et al. (2007). Table 1 gives a log of the observations.

All three of the data sets were reduced using the techniques described in Carr & Najita (2008). The GTO data set lacks off-target frames and consists of just one exposure in each of the nod positions. In this case, the identification of bad pixels relied solely on the inspection of the single images, using a comparison of the two nod positions as an aid. The spectra were calibrated by creating a spectral response function from a suite of archival

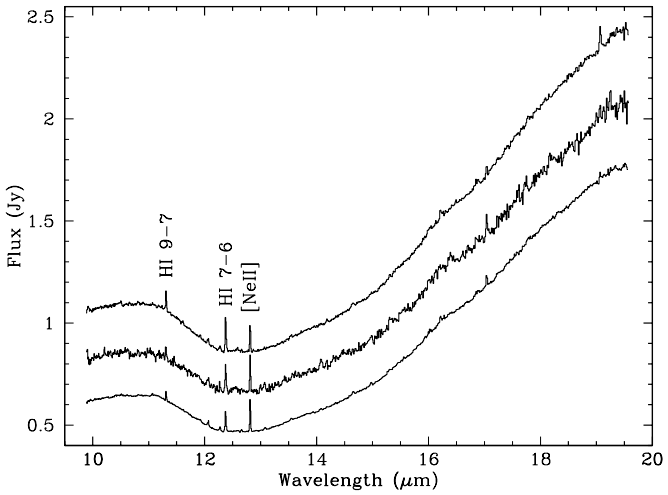

Figure 1. *Spitzer* IRS short-high spectra of TW Hya taken at three epochs: SH1 (top), SH2 (bottom), and the GTO spectrum (middle). The GTO spectrum is offset by +0.15 Jy and SH1 by +0.25 Jy for clarity.

Table 2
Continuum and Errors

Feature	Wavelength	GTO		SH1		SH2	
		Continuum	Error	Continuum	Error	Continuum	Error
	(μm)	(Jy)	(Jy)	(Jy)	(Jy)	(Jy)	(Jy)
H I 9–7	11.31	0.68	0.013	0.81	0.0037	0.62	0.0019
Ne II	12.81	0.51	0.011	0.61	0.0030	0.47	0.0017
CO_2	14.97	0.76	0.015	0.89	0.0036	0.69	0.0019
H2 *S*(1)	17.03	1.28	0.023	1.47	0.0063	1.18	0.0050
H I 8–7	19.06	1.85	0.029	2.09	0.012	1.70	0.0084

standard star spectra reduced in the same way as the target spectra. The spectral response function was customized for each nod position of each data set by combining those standard star spectra that minimized the fringing in order 20. Subsequent application of IRSFRINGE (Lahuis et al. 2006a) found little residual fringing. Table 2 provides estimates of the resulting noise per pixel and the continuum level at the wavelengths of selected spectral features in the 10–20 μm range. The noise in each spectral region was estimated from the difference of the spectra taken in the "A" and "B" beam positions at each epoch.

3. RESULTS

3.1. Continuum and Emission Lines

The shape of the mid-infrared continuum is similar in all three spectra (Figure 1). The continuum in the GTO spectrum is well approximated by 1.1 times the flux of the continuum in SH2. The SH1 continuum is approximately 1.3 times the SH2 continuum, although it is shallower in slope than SH2 beyond ∼15 μm. These differences may arise in part from pointing errors (<20% photometric uncertainty in SH for the nominal *Spitzer* pointing accuracy; see *Spitzer* Observer's Manual, ver. 8.0) or true variability in the T Tauri continuum (e.g., Muzerolle et al. 2009) or a combination of these. The [Ne II] line at 12.81 μm and H I lines at 11.31 μm and 12.37 μm are strongly in emission at each epoch.

Notably, in none of the three epochs does TW Hya show strong mid-infrared molecular emission like that seen in *Spitzer* spectra of classical T Tauri stars that have been reported in the literature (Carr & Najita 2008; Salyk et al. 2008; see also

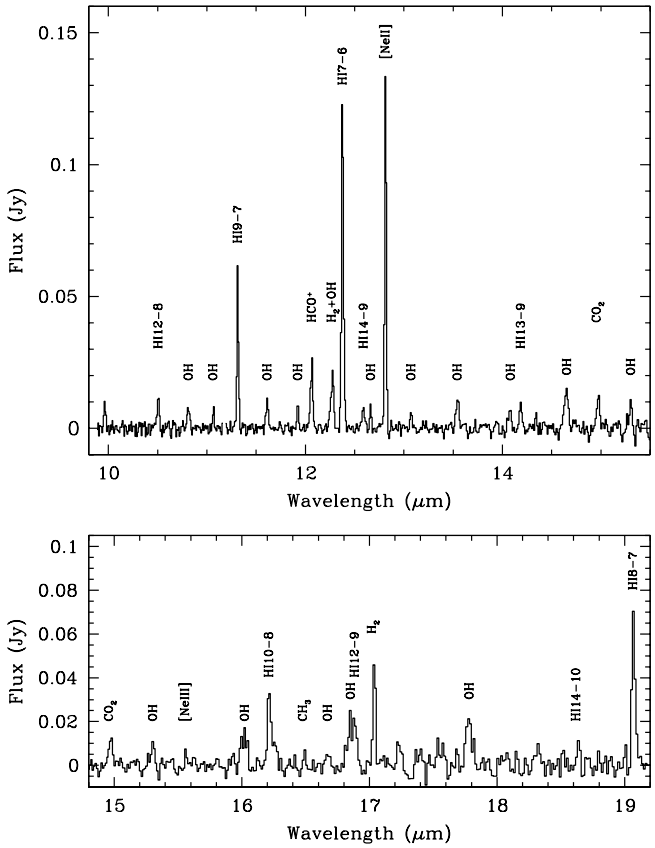

Figure 2. Average of the SH1 and SH2 spectra of TW Hya from which a polynomial fit to the continuum has been subtracted. Emission features of atomic lines (H I, [Ne II], and possibly [Ne III]) and molecules (H_2, OH, CO_2, HCO^+, and possibly CH_3) are detected. The [Ne III] and CH_3 features are clearer in the SH2 and SH1 spectra, respectively (see Figure 3).

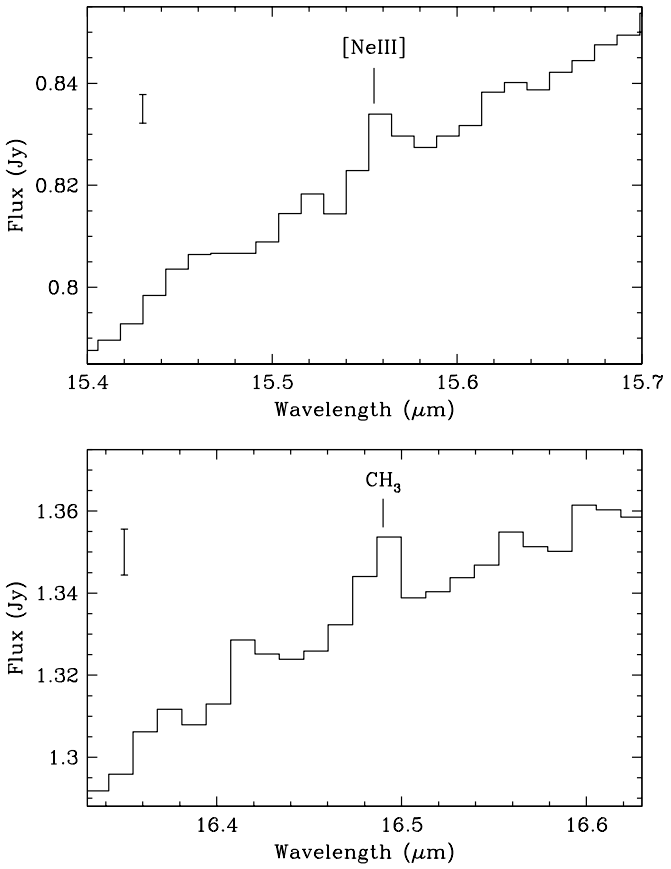

Figure 3. Region around the [Ne III] line in the SH2 spectrum (top) and the CH_3 emission band in the SH1 spectrum (bottom). A representative error bar ($\pm 1\sigma$) is shown in the upper left corner of each panel.

Pascucci et al. 2009). The [Ne II] line luminosity is a convenient reference, since TW Hya and AA Tau (Carr & Najita 2008) have similar [Ne II] line luminosities, within a factor of 2. In AA Tau, the molecular emission is stronger than the [Ne II] emission, whereas in TW Hya, the [Ne II] emission is, by far, one of the brightest lines in the spectrum.

Nevertheless, TW Hya does show a rich spectrum of weaker emission features. To illustrate this, we show in Figure 2 the average of SH1 and SH2 after subtracting a high-order polynomial fit to the continuum. The features that are seen correspond well in wavelength with known atomic lines (H I, Ne II, and Ne III) and other molecular features (H_2, OH, CO_2, HCO^+, and possibly CH_3). The transitions that dominate the detected OH features are listed in Table 3. The CO_2 band has been detected both in emission (Carr & Najita 2008; Salyk et al. 2008) and in absorption (e.g., Lahuis et al. 2006b) from T Tauri stars.

We identify the feature at 12.06 μm as the ν_2 fundamental Q-branch of HCO^+ (Davies & Rothwell 1984). The detection of HCO^+ emission is interesting, and to our knowledge this band has not been reported previously in any young stellar object (YSO). There is also a weak feature observed in the SH1 spectrum at 16.48 μm that may be the ν_2 Q-branch of the fundamental band of CH_3 (Bezard et al. 1999; Feuchtgruber et al. 2000). In addition, the [Ne III] line is marginally detected in the SH2 spectrum. Figure 3 gives an expanded view of the region around the weak features [Ne III] and CH_3 in the epoch in which they were detected (SH2 and SH1, respectively). These features are more apparent in the individual spectra than in the average of SH1 and SH2 (Figure 2).

Table 3
OH Features Detected

λ (μm)	v	Transitions
10.81	0	3/2 R 29.5, 1/2 R 28.5
11.06	0	3/2 R 28.5, 1/2 R 27.5
11.31	0	3/2 R 27.5, 1/2 R 26.5
11.61	0	3/2 R 26.5, 1/2 R 25.5
11.92	0	3/2 R 25.5, 1/2 R 24.5
12.65	0	3/2 R 23.5, 1/2 R 22.5
13.08	0	3/2 R 22.5, 1/2 R 21.5
13.54	0	3/2 R 21.5, 1/2 R 20.5
14.08	0	3/2 R 20.5, 1/2 R 19.5
14.65	0	3/2 R 19.5, 1/2 R 18.5
	1	3/2 R 20.5, 1/2 R 19.5
15.30	0	3/2 R 18.5, 1/2 R 17.5
	1	3/2 R 19.5, 1/2 R 18.5
16.02	0	3/2 R 17.5, 1/2 R 16.5
16.84[a]	0	3/2 R 16.5, 1/2 R 15.5
17.78	0	3/2 R 15.5, 1/2 R 14.5

Note. [a] Blended with the H I 12–9 line.

Since fitting and subtracting a high-order polynomial can affect the strength of weak features (e.g., if it incorrectly fits the local continuum), we did not measure line strengths from the continuum-subtracted spectrum. We instead used the continuum-subtracted spectrum to identify the approximate wavelengths of features to be fit, and we then measured feature strengths from the original spectrum. We made a least-squares fit to each feature using a model of a Gaussian and a quadratic approximation to the local continuum. A Marquardt routine was

Table 4
Emission Line Properties in the SH1 Spectrum

Feature	λ	Flux	Err	FWHM	+Err	−Err	EW	Err
	(μm)	(10^{-14} erg s^{-1} cm^{-2})		(10^{-2} μm)			(10^{-3} μm)	
H I 12–8	10.502	1.07	0.54	2.2	2.1	0.9	0.47	0.24
OH	10.809	0.82	0.51	2.8	3.5	1.9	0.38	0.24
OH	11.077	1.26	0.73	5.1	5.2	2.4	0.62	0.36
H I 9–7	11.310	3.74	0.38	1.6	0.2	0.1	1.96	0.20
OH	11.609	0.69	0.40	2.0	1.9	1.2	0.42	0.24
OH	11.922	0.66	0.30	1.8	1.6	0.7	0.46	0.21
HCO^+	12.064	1.51	0.41	2.8	1.1	0.6	1.13	0.31
$H_2S(2)$+OH	12.276	1.49	0.42	3.4	1.4	0.9	1.22	0.34
H I 7–6	12.374	8.10	0.33	2.1	0.9	1.2	6.75	0.28
H I 14–9	12.587	0.51	0.25	1.5	1.6	0.7	0.43	0.21
OH	12.663	0.37	0.28	1.3	2.0	0.7	0.33	0.25
Ne II	12.814	4.95	0.29	1.8	0.1	0.1	4.43	0.26
OH	13.069	0.26	0.19	1.3	2.4	0.9	0.23	0.18
OH	13.541	0.80	0.33	3.4	1.9	0.9	0.73	0.30
OH	14.074	0.31	0.23	2.3	4.7	1.9	0.28	0.20
H I 13-9	14.183	0.89	0.30	3.1	1.6	1.2	0.79	0.27
OH	14.645	1.23	0.42	4.7	2.1	1.4	1.06	0.36
CO_2	14.974	0.70	0.47	5.4	6.1	3.5	0.59	0.39
OH	15.302	0.43	0.26	1.7	2.4	0.9	0.34	0.21
OH	16.013	1.56	0.59	6.4	4.2	1.6	1.12	0.42
H I 10–8	16.215	1.78	0.51	3.8	1.4	1.2	1.23	0.36
CH_3	16.482	0.45	0.33	1.9	4.7	1.6	0.30	0.23
H I 12–9+OH	16.859	2.53	0.74	8.0	3.5	2.1	1.69	0.49
H_2 $S(1)$	17.036	1.21	0.41	2.0	1.2	0.5	0.79	0.27
OH	17.762	1.38	0.57	4.7	2.6	2.1	0.84	0.35
H I 8–7	19.064	3.06	0.83	3.1	0.9	0.9	1.77	0.48

used to find the best fit (e.g., Bevington 1969). Estimated errors on the line fluxes and line widths were found by determining the range of values enclosed by the 68% confidence interval (a "1σ" estimate) that is appropriate for the six parameters in the fit (e.g., Lampton et al. 1976).

Tables 4 and 5 report the fluxes, Gaussian widths, and equivalent widths of the features in the SH1 and SH2 spectra, respectively. Table 6 reports the fluxes and equivalent widths measured from fits to the features in the GTO spectrum. Feature widths are not reported for the GTO spectrum because they are not well constrained given the lower signal to noise of that spectrum. The fluxes of the features measured in the GTO spectrum (H I 9–7, H I 7–6, [Ne II], H_2, and HCO^+) are consistent within the errors with the fluxes measured in SH1 and SH2.

3.2. Properties and Variability of Emission Features

For the lines that appear to be unblended (i.e., the H I lines 12–8 at 10.5 μm, 9–7 at 11.31 μm, 7–6 at 12.37 μm, 13–9 at 14.18 μm, 8–7 at 19.07 μm, [Ne II] at 12.81 μm, and the H_2 S1 line), the line center positions are typically within ± 50 km s^{-1} of their rest values. As shown in Figure 4, the widths of these lines are, for the most part, consistent with being spectrally unresolved.

We detect a series of OH features that are each comprised of multiple pure rotational transitions of OH. Table 3 gives the approximate wavelengths of these OH groups and the transitions that dominate the flux we observe. Most of the emission arises from transitions within the $v = 0$ ground vibrational state, from both the $^2\Pi_{3/2}$ and $^2\Pi_{1/2}$ rotational ladders, with $J = 14.5$ to $J = 29.5$. Figure 3 of Tappe et al. (2008) gives a graphical illustration of the range of upper energy levels probed by these transitions. Some low-lying $v = 1$ transitions may also

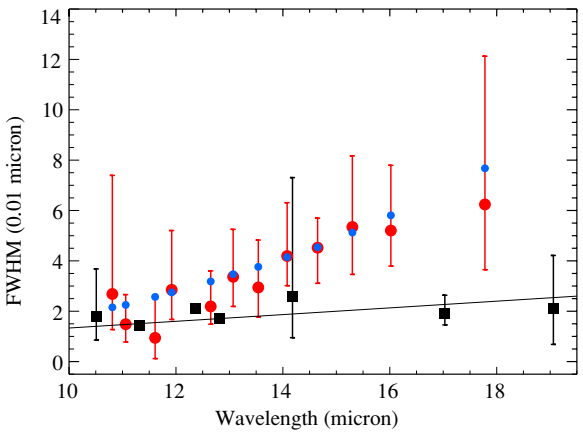

Figure 4. FWHM of the Gaussian fits to OH features (large red dots) and [Ne II] and unblended H I lines (black squares) in the SH2 spectrum. Where error bars are not apparent, they are smaller than the size of the symbol. The nominal resolution of IRS in the short-high mode ($R = 750$; black line) is shown for comparison. While the H I and [Ne II] lines are spectrally unresolved, the widths of the OH features grow with wavelength due to the increasing spread in the wavelengths of individual OH lines that make up a given feature. This is illustrated by the agreement with the small blue dots, which show this spread in wavelengths added in quadrature with the spectral resolution at the central wavelength of each feature.

(A color version of this figure is available in the online journal.)

contribute by enhancing the $v = 0$ emission groups when there is a wavelength coincidence (e.g., at 14.65 μm and 15.30 μm). The widths of the OH features are comparable to or broader than the nominal spectral resolution of IRS; e.g., the features at 14.08 μm, 14.65 μm, 15.30 μm, 16.02 μm, and 17.78 μm are spectrally resolved (Figure 4). The increase in the feature widths with wavelength arises because the spread in the wavelengths of

Table 5
Emission Line Properties in the SH2 Spectrum

Feature	λ	Flux	Err	FWHM	+Err	−Err	EW	Err
	(μm)	(10^{-14} erg s^{-1} cm^{-2})		(10^{-2} μm)			(10^{-3} μm)	
H I 12-8	10.508	0.45	0.24	1.8	1.9	0.9	0.26	0.14
OH	10.8146	0.38	0.26	2.7	4.7	1.4	0.23	0.16
OH	11.063	0.43	0.20	1.5	1.2	0.7	0.27	0.12
H I 9–7	11.310	1.60	0.19	1.4	0.2	0.2	1.10	0.13
OH	11.614	0.15	0.13	0.9	1.6	0.8	0.12	0.11
OH	11.922	0.52	0.23	2.9	2.4	1.2	0.47	0.21
HCO^+	12.064	1.32	0.21	2.6	0.5	0.6	1.30	0.20
$H_2S(2)$+OH	12.276	1.14	0.20	2.9	0.7	0.7	1.21	0.21
H I 7–6	12.373	4.53	0.20	2.1	0.1	0.1	4.92	0.21
OH	12.659	0.45	0.19	2.2	1.4	0.7	0.52	0.21
Ne II	12.813	5.56	0.16	1.72	0.0	0.1	6.47	0.19
OH	13.081	0.55	0.21	3.4	1.9	1.2	0.65	0.25
OH	13.547	0.48	0.20	2.9	1.9	1.2	0.56	0.23
OH	14.070	0.62	0.23	4.2	2.1	1.2	0.72	0.26
H I 13–9	14.181	0.20	0.18	2.6	4.7	1.6	0.23	0.21
OH	14.651	0.94	0.22	4.5	1.2	1.4	1.04	0.25
CO_2	14.972	0.62	0.17	2.7	1.1	0.6	0.67	0.19
OH	15.294	0.75	0.28	5.4	2.8	1.9	0.77	0.29
Ne III	15.558	0.25	0.19	1.6	2.1	1.2	0.24	0.18
OH	16.016	1.01	0.35	5.2	2.6	1.4	0.92	0.32
H I 10–8	16.212	0.88	0.26	2.6	1.2	0.7	0.77	0.23
H I 12–9+OH	16.861	1.69	0.58	8.0	3.8	2.1	1.41	0.48
H_2 $S(1)$	17.035	1.26	0.31	1.9	0.7	0.5	1.03	0.25
OH	17.767	1.08	0.57	6.2	5.9	2.6	0.82	0.43
H I 8–7	19.061	0.71	0.50	2.1	2.1	1.4	0.50	0.35

Table 6
Emission Line Properties in the GTO Spectrum

Feature	λ	Flux	Err	EW	Err
	(μm)	(10^{-14} erg s^{-1} cm^{-2})		(10^{-3} μm)	
H I 9–7	11.306	2.92	1.53	1.83	0.96
HCO^+	12.060	2.39	1.44	2.12	1.28
H_2 $S(2)$	12.272	1.55	1.00	1.51	0.97
H I 7–6	12.372	7.13	1.37	7.13	1.37
Ne II	12.812	5.90	0.91	6.29	0.97

the lines that contribute to each feature is progressively larger at longer wavelengths.

Figure 5 shows the ratio of the line fluxes, equivalent widths, and Gaussian line widths in SH1 compared to SH2. The flux of the [Ne II] line is similar in the two epochs (within ∼10%), but its equivalent width is lower (by ∼30%) in SH1 than in SH2 because of the brighter continuum in SH1 (Figure 1). In comparison, the H I lines at 11.31 μm and 12.37 μm are stronger in both flux (by a factor of ∼2) and equivalent width (by ∼30%) in SH1 compared to SH2. The variation of the H I lines suggests true variability. Neither the 12.37 μm H I line nor the [Ne II] line is spatially extended with respect to the continuum at the spatial resolution of *Spitzer*; hence, while a small pointing error could alter the measured line flux, it is unlikely to alter the line equivalent width. The 12.37 μm line is brighter than the [Ne II] line in SH1 and fainter than [Ne II] in SH2, also indicating true variability. The H_2 lines have similar fluxes in both epochs, as does HCO^+.

Some features are apparent in one epoch but not the other. We find in SH2, but not SH1, a weak feature at the wavelength of the [Ne III]15.55 μm line. The [Ne III] line may be more apparent in SH2 because of the higher signal to noise of the SH2 spectrum. We find in SH1, but not SH2, weak features at the wavelength of the CH_3 band (at 16.48 μm) and the H I 14–9 line (at 12.58 μm). Finding the latter feature in SH1 but not the higher signal-to-noise SH2 is consistent with the brighter emission observed for the dominant H I lines (7–6 and 9–7) in SH1 than in SH2 (Figure 1).

3.3. H I Lines

The flux of the H I 7–6 line, as an average of the flux in SH1 (2.3×10^{28} erg s^{-1}) and SH2 (1.3×10^{28} erg s^{-1}), is in good agreement with the H I 7–6 flux of 1.7×10^{28} erg s^{-1} reported by Ratzka et al. (2007).

The relative fluxes of the H I lines in SH1 and SH2 can be accounted for roughly with case B recombination. Figures 6 and 7 compare the H I fluxes measured in SH1 and SH2, respectively, with the relative fluxes for case B at a temperature of $T = 10^4$ K and an electron density of $n_e = 10^4$ cm^{-3} (Storey & Hummer 1995). The case B relative fluxes are similar (i.e., within our measurement errors) over a broad range in temperature (1000–20,000 K) and electron density ($n_e = 10^3$–10^8 cm^{-3}). As a result, the relative fluxes we measure do not constrain the temperature and electron density of the emitting gas.

In comparison, greater variation is expected in the relative line fluxes of lower lying H I lines over the same range in density and temperature. As described by Bary et al. (2008), the Paschen (Paβ, Paγ, Paδ, and 8 through 14) and Brackett (Brγ and 10 through 16) lines of T Tauri stars that originate from the same range of upper energy levels also show line ratios consistent with case B recombination. They interpret their line ratios as favoring low temperature ($\lesssim$2000 K) and high electron density (10^9 cm^{-3} $< n_e \lesssim 10^{10}$ cm^{-3}).

The mid-infrared (MIR) lines we observe are predicted to have inverted populations at such high densities (Hummer &

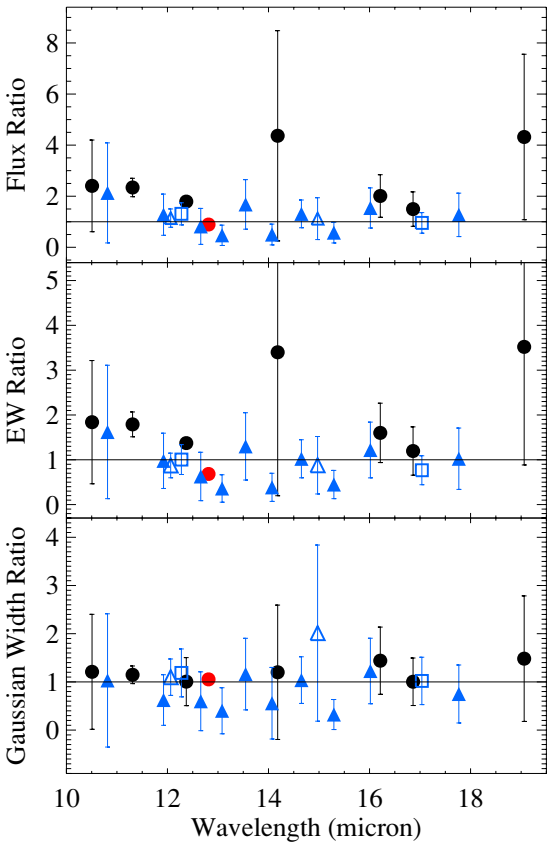

Figure 5. Ratio of line fluxes (top), equivalent widths (middle), and Gaussian FWHM (bottom) in SH1 compared to SH2 for H I (black dots), [Ne II] (red dot), H_2 (open blue squares), OH (solid blue triangles), and HCO^+ and CH_3 (open blue triangles). The fluxes of the H I lines are larger by ∼2 in flux in SH1 compared to SH2. The equivalent width of the [Ne II] line is smaller in SH1 than SH2.

(A color version of this figure is available in the online journal.)

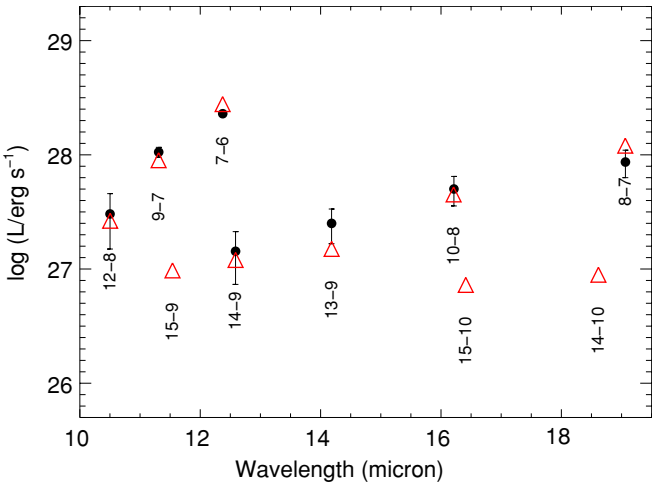

Figure 6. H I line luminosities from the SH1 spectrum (dots with error bars) compared with relative fluxes from case B recombination (triangles). The H I 15–9, H I 15–10, and H I 14–10 lines are not detected, consistent with their low anticipated fluxes.

(A color version of this figure is available in the online journal.)

Storey 1987). Transitions between high-lying levels typically become inverted at lower densities than those between low-lying levels. So, for example, the H I 9–7 and 8–7 transitions have a population inversion at densities above $n_e \sim 10^8$ cm^{-3},

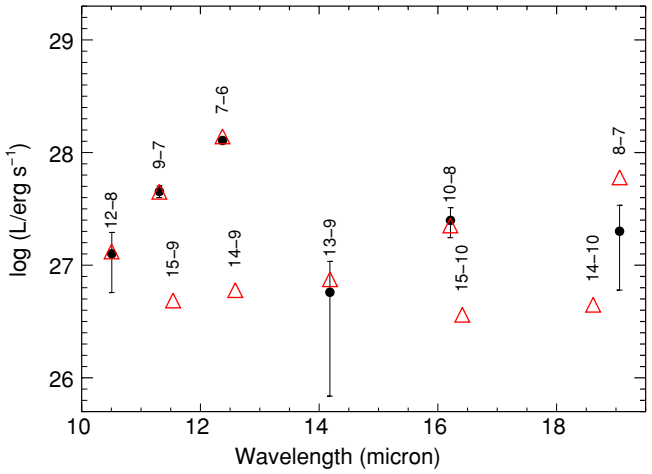

Figure 7. H I line luminosities from the SH2 spectrum (dots with error bars) compared with relative fluxes from case B recombination (triangles). The H I 8–7 line is weaker at this epoch and not in as good agreement with the case B relative fluxes. The H I 15–9, H I 14–9, H I 15–10, and H I 14–10 lines are not detected, consistent with their low anticipated fluxes.

(A color version of this figure is available in the online journal.)

whereas the H I 7–6 transition is inverted at higher densities ($n_e \gtrsim 10^8$–10^9 cm^{-3}) and the H I 13–9 transition at lower densities ($n_e \gtrsim 10^7$ cm^{-3}). The fact that the relative fluxes we observe in TW Hya are consistent with case B recombination suggests that we are not seeing maser emission in this source, as the predicted amplification factors can differ widely between transitions. Similarly, MIR H I transitions were not found to be masing in a study of MWC349 (Smith et al. 1997), a source that shows maser emission in longer wavelength H I lines.

We can estimate the number of ionizing photons that are needed to produce the observed H I emission under the assumption of ionization equilibrium, i.e., that the number of ionizations per second equals the number of recombinations per second. Since the recombination line luminosity $L_{\rm ul} = n_e n_p \epsilon_{\rm ul} V$ (where V is the optically thin emitting volume, n_e is the electron density, and $\epsilon_{\rm ul}$ is the emissivity of the transition in erg s^{-1} cm^3), the total recombination rate $\alpha_B n_e n_p V$ can be expressed as $\alpha_B L_{\rm ul}/\epsilon_{\rm ul}$. For the H I 9–7 transition at 11.31 μm in SH2, $L_{\rm ul} = 4.5 \times 10^{27}$ erg s^{-1}. From Hummer & Storey (1987), $\epsilon_{\rm ul} = 3.7 \times 10^{-28}$ erg s^{-1} cm^3, and $\alpha_B = 2.6 \times 10^{-13}$ cm^{3}s^{-1} for $T_e = 10^4$ K and $n_e = 10^4$ cm^{-3}. For these values, the total recombination rate is 3.2×10^{42} s^{-1}.

In comparison, the ionizing photon flux of T Tauri stars is often estimated as 10^{41} s^{-1} (e.g., Hollenbach et al. 2000), although Alexander et al. (2005) derived ionizing photon fluxes of 10^{41}–10^{44} s^{-1} for various T Tauri stars based on CIV λ1549 line luminosities. Looking at the situation for TW Hya itself, Herczeg (2007) estimated an ionizing photon flux of 5×10^{41} s^{-1} from the accretion shock onto the star based on the observed X-ray and FUV line fluxes and the assumption of collisional ionization, with a factor of 5 uncertainty in the quoted value. The number of ionizing photons that we infer is at the upper end of this range, so TW Hya may emit enough ionizing photons to explain the mid-infrared H I line fluxes that we observe. However, if the EUV photons are sufficient to produce the mid-infrared H I line fluxes, they are likely to produce more [Ne II] or [Ne III] emission than is observed (Hollenbach & Gorti 2009; see also below).

We can also estimate the mass of the emitting (ionized) gas, under the assumption of optically thin emission and

constant density. The mass of ionized hydrogen is $m_H\, n_p\, V = (m_H/n_e)(L_{\rm ul}/\epsilon_{\rm ul}) = 1.6 \times 10^{31}$ g cm$^{-3}/n_e$. This corresponds to a total number of hydrogen atoms of 10^{55} cm$^{-3}/n_e$. If we require $n_e \lesssim 10^8$ cm^{-3} to avoid inverted populations, the emitting mass of ionized gas is $\gtrsim 10^{23}$ g. In Section 4, we consider the region of the YSO system in which such emission might arise.

3.4. Neon Lines

The range of [Ne II] equivalent widths we measure is consistent with the equivalent width reported for this line from ground-based high-resolution spectroscopy. We measure equivalent widths of 63 ± 10 Å, 44 ± 3 Å, and 65 ± 2 Å in the GTO, SH1, and SH2 spectra, respectively. In comparison, Herczeg et al. (2007) measured at high spectral resolution an equivalent width of 62 ± 11 Å for the [Ne II] line using MICHELLE on Gemini. TW Hya was also studied at high spectral resolution by Pascucci & Sterzik (2009) using VISIR on the VLT. They measured a [Ne II] equivalent width of 41 Å and a flux of 3.8×10^{-14} erg s^{-1} cm^{-2}, within 65%–75% of the flux of 5.9×10^{-14} erg s^{-1} cm^{-2}, 5.0×10^{-14} erg s^{-1} cm^{-2}, and 5.6×10^{-14} erg s^{-1} cm^{-2} measured for the GTO, SH1, and SH2 spectra, respectively.

Time variability, pointing errors, flux calibration issues, and/or the narrower slit of the ground-based observations may account for any differences between the IRS and ground-based results. In particular, the 0.″4 slit of the VISIR observations translates into a physical size scale of ±10 AU at the 50 pc distance of TW Hya. As noted by Pascucci & Sterzik (2009), if the [Ne II] emission arises from a disk, the narrow slit may exclude a reasonable fraction of the emission, since Glassgold et al. (2007) have shown that the [Ne II] emitting region of the disk may extend out to a radius of ∼20 AU. We further note here that in the calculations of Meijerink et al. (2008) for their fiducial T Tauri disk, ∼75% of the [Ne II] emission arises from within 10 AU. If there is no substantial gaseous disk within the optically thin region of the TW Hya disk (e.g., if the disk is dynamically cleared by an orbiting planet), then it would be more appropriate to look at the emission arising from 4–10 AU. The fraction of the [Ne II] emission that arises from this region of the disk is ∼65%, comparable to the fraction of the IRS [Ne II] flux that is recovered in the VISIR data.

The MICHELLE observations of Herczeg et al. (2007) were also made with a 0.″4 slit, but in poor seeing. So slit losses may be an issue there, but the observations are likely to be less sensitive to a difference in the spatial extent of the [Ne II] emission relative to the MIR continuum. That is, the equivalent width of the observations could be similar to that measured by *Spitzer*, as observed. Near-simultaneous narrow- and wide-slit ground-based [Ne II] observations of TW Hya, taken in good seeing, would be useful in constraining the spatial extent of the emission.

While [Ne II] is commonly detected from T Tauri stars (Pascucci et al. 2007; Espaillat et al. 2007; Lahuis et al. 2007; Ratzka et al. 2007; Guedel et al. 2008, 2009; Flaccomio et al. 2009), [Ne III] is rarely detected, with upper limits typically an order of magnitude lower (e.g., Lahuis et al. 2007). In addition to our possible detection of [Ne III] from TW Hya, the T Tauri stars Sz 102 and WL5 also show [Ne III] emission. Sz 102 has neon fluxes and a [Ne III]/[Ne II] ratio (∼0.06; Lahuis et al. 2007) that are similar to the values reported here for TW Hya ([Ne III]/[Ne II] ∼0.045). In contrast to TW Hya, Sz 102 drives a jet (e.g., Coffey et al. 2004, where the source is known as TH 28), so its neon emission may have contributions from a both a disk and a jet. [Ne III] is also detected from WL5, where the [Ne III]/[Ne II] flux ratio is much higher, ∼0.25 (Flaccomio et al. 2009).

The [Ne II] and [Ne III] line fluxes that we detect from TW Hya are in good agreement with predictions for gaseous disk atmospheres that are irradiated by stellar X-rays. For an X-ray luminosity of 2×10^{30} erg s^{-1}, which is roughly the X-ray luminosity of TW Hya (Kastner et al. 1999; Robrade & Schmitt 2006), the models of Glassgold et al. predict a [Ne II] luminosity of 1.4×10^{28} erg s^{-1} and a [Ne III] luminosity of 1.6×10^{27} erg s^{-1}. In comparison, we measure [Ne II] and [Ne III] luminosities of 1.6×10^{28} erg s^{-1} and 0.7×10^{27} erg s^{-1} in the SH2 spectrum. In the Glassgold models, the [Ne III]/[Ne II] ratio is small because the emission arises in a region with a significant abundance of neutral hydrogen atoms (the ionization fraction $x_e \simeq 0.001$). As a result, there is efficient charge exchange between Ne III and H I and a consequent reduction in the Ne III abundance.

EUV photons reaching the disk would enhance the neon emission above that produced by X-ray irradiation. For an EUV irradiated region, which is typically fully ionized ($x_e \sim 1$), Hollenbach & Gorti (2009) find that a small [Ne III]/[Ne II] ratio can be produced with a soft EUV spectrum, e.g., a blackbody with a temperature of 30,000 K. A harder spectrum, e.g., with constant νL_ν, would produce [Ne III]/[Ne II] ∼1, in conflict with the observations. The EUV spectrum of TW Hya has not been measured directly, although Herczeg (2007) has estimated a significant EUV flux from the accretion column based on the observed FUV and soft X-ray spectrum. Herczeg did not comment on the spectral shape of the predicted EUV emission. The impact of the emitted EUV on the disk may be limited by foreground H I absorption (e.g., in a magnetosphere; Alexander et al. 2004). Reviewing the literature, Herczeg (2007) estimated that only a small fraction of the EUV (equivalent to 10^{39} photons s^{-1}) reaches the disk. So the EUV contribution to the neon emission from the disk may be limited.

3.5. Molecules

The OH features we detect originate from very high energy levels (upper energy levels 6,000–23,000 K above ground) and have large transition probabilities (A-values of 20–70 s^{-1}). OH emission from other young stellar disks has been reported previously for lower rotational lines in both the ground vibrational state (Carr & Najita 2008) and the fundamental ro-vibrational band (Mandell et al. 2008; Salyk et al. 2008). The rotational temperatures derived for the emission from these *lower* rotational levels are consistent with thermal OH emission at 500–1000 K. The much *higher* energy rotational states observed in emission in the SH spectrum of TW Hya are more similar to the superthermal OH emission detected by Tappe et al. (2008) in the *Spitzer* IRS spectrum of young stellar outflow HH 211.

One possible interpretation of the highly excited OH emission detected from TW Hya is that it arises from gas that is hot and dense enough to collisionally populate the upper levels. The excitation conditions for such thermal OH emission would exceed even those for the CO fundamental emission observed from TW Hya (upper energy levels 3000–6000 K and A-values ∼10 s^{-1}), which arises from gas at ∼1000 K in the inner 1 AU of the disk (Salyk et al. 2007). The ro-vibrational transitions of CO are generally considered to be a good tracer of hot and dense molecular gas in the circumstellar environment, and the lack of a CO component corresponding to the hotter OH emission is curious.

The lack of H_2O emission, along with a highly excited OH emission spectrum, is a striking difference between TW Hya and normal classical T Tauri stars. However, close examination of the IRS SH spectra of classical T Tauri stars does reveal the presence of these same OH emission features (J. S. Carr & J. R. Najita 2010, in preparation), with rotational temperatures ∼4000 K. This emission was not previously recognized because of the complexity of the dense H_2O emission in which the OH emission is embedded. Hence, the character of the OH emission in TW Hya and that of a classical T Tauri star such as AA Tau may be more similar than would appear at first glance.

A likely possibility is that such highly excited OH emission arises from the photodissociation of H_2O, which is also the interpretation given by Tappe et al. (2008) for the OH emission from HH 211. The photodissociation of H_2O by UV photons in the second absorption band of water (λ = 1200–1400 Å) will produce OH molecules in highly excited rotational levels but predominantly in the ground vibrational state (Harich et al. 2000). We will present a detailed analysis of the OH spectrum of TW Hya in a following paper.

The H_2 emission that we observe is much weaker than either the [Ne II] or H I 7–6 emission from TW Hya. The line luminosities are in the range found for other accreting young stars. In the ground-based (IRTF/TEXES) H_2 survey of Bitner et al. (2008), the H_2 S(2) line luminosity of a low mass star such as GV Tau N is $\sim 3 \times 10^{-6}\, L_\odot$, although upper limits on the $S(2)$ line luminosity for some T Tauri stars are much lower (e.g., $\sim 0.4 \times 10^{-6}\, L_\odot$ for LkCa 15). In comparison, the line luminosities of the $S(1)$ and $S(2)$ emission that are detected from TW Hya in SH2 are $0.8 \times 10^{-6}\, L_\odot$ and $0.5 \times 10^{-6}\, L_\odot$, respectively. Since the $S(2)$ line of TW Hya is blended with an OH feature, we assumed an OH contribution that is similar to that of neighboring OH features in estimating the flux of the $S(2)$ line. The observed $S(1)$ luminosity is similar to the value of $0.2 \times 10^{-6}\, L_\odot$ that is predicted for TW Hya by Gorti & Hollenbach (2008).

Interestingly, the H_2 emission from TW Hya is stronger than the upper limits on the H_2 flux that Bitner et al. (2008) measured for TW Hya. Whereas we measure line fluxes of 1.3×10^{-14} erg s^{-1} cm^{-2} and 0.6×10^{-14} erg s^{-1} cm^{-2} for the $S(1)$ and $S(2)$ lines (5σ and 3σ detections, respectively, in SH2), Bitner et al. (2008) provide 3σ upper limits for the $S(1)$ and $S(2)$ lines of 0.7×10^{-14} erg s^{-1} cm^{-2} and 0.6×10^{-14} erg s^{-1} cm^{-2}, respectively. Perhaps the narrower slit (0.″81 and 0.″54 for the S1 and S2 lines, respectively) of the TEXES measurements plays a role here as well. The line widths that are measured for H_2 emission from young stars, when it is detected by TEXES in more distant sources (∼140 pc), are ∼10 km s^{-1}, which is consistent with much of the emission arising from the 10–50 AU region of the disk. As discussed in the context of the [Ne II] emission from TW Hya (Section 3.4), much of this region of the disk is excluded by the narrow slit in a nearby source such as TW Hya. As in the case of [Ne II], near-simultaneous narrow- and wide-slit ground-based observations of the H_2 emission from TW Hya, taken in good seeing, would be useful in constraining the spatial extent of the emission.

We also detect molecules other than OH and H_2 in the TW Hya spectrum (CO_2, HCO^+, and possibly CH_3). The properties of these emission features will be discussed in greater detail in a future publication.

4. DISCUSSION

4.1. Evolutionary State of the TW Hya Disk

As a well-studied, nearby transition object, TW Hya has been a touchstone for understanding the origin and evolutionary state of such systems. Transition objects have unusual SEDs characterized by a deficit of infrared excess at short wavelengths, a trait that is interpreted as indicating that the disk is optically thin in the continuum within a given radius $R_{\rm hole}$ (Strom et al. 1989). Analyses of SEDs of transition objects find $R_{\rm hole}$ values of a few AU to ∼50 AU in some cases (Espaillat et al. 2007). In comparison, the SED of TW Hya indicates that its disk is optically thin within ∼4 AU of the star (Calvet et al. 2002; Uchida et al. 2004). An inner hole in the dust continuum emission is detected at 7 mm and at 10 μm (Hughes et al. 2007; Ratzka et al. 2007).

Such a dust distribution could be interpreted as a result of grain growth (Strom et al. 1989; Dullemond & Dominik 2005), photoevaporation (Clarke et al. 2001; Alexander et al. 2006; Gorti & Hollenbach 2009; Owen et al. 2010), or a gap opened by an orbiting giant planet (e.g., Marsh & Mahoney 1992; Calvet et al. 2002, 2005; Rice et al. 2003; Quillen et al. 2004). These scenarios could potentially be distinguished by examining properties other than the SED, since the scenarios make different predictions for the stellar accretion rate, disk mass, and radial distribution of gas in the disk (Najita et al. 2007b; Alexander & Armitage 2007).

The first two diagnostics (stellar accretion rates and disk masses) were used by Najita et al. (2007b) to probe the nature of transition objects in the Taurus star-forming region. They found that Taurus transition objects have higher than average disk masses as well as stellar accretion rates that are ∼10 times lower than non-transition objects. These properties are roughly consistent with the predictions of theories of giant planet formation (e.g., Lubow et al. 1999; Lubow & D'Angelo 2006). The high disk mass of TW Hya ($>0.06\, M_\odot$; Calvet et al. 2002) and its comparatively low stellar accretion rate ($\sim 10^{-9}\, M_\odot$ yr^{-1}; e.g., Herczeg et al. 2004; Muzerolle et al. 2000; Alencar & Basri 2000) place it in a similar region of the $\dot{M}$–$M_{\rm disk}$ plane as the Taurus transition objects.

Studies of line emission from the gaseous component of transition disks, like that presented here, offer the opportunity to complement studies of stellar accretion rates and disk mass, by probing the radial distribution of gas in the disk and therefore the evolutionary state of the system. As described by Najita et al. (2007b, 2008):

1. In the grain growth and planetesimal formation scenario, the inner disk is rendered optically thin in the continuum, but the gaseous component is unaltered and would fill the region within $R_{\rm hole}$. Emission from gas *everywhere* within $R_{\rm hole}$ would produce bright emission because of the lack of continuum emission from same region of the disk.
2. If a planet has formed with a mass sufficient to open a gap ($\sim 1 M_J$), gas will be cleared in the vicinity of its orbit, but gap-crossing streams, from the outer disk to the planet, and from the planet to the inner disk, can allow continued accretion onto both the planet and the star, the latter via the replenishment of the inner disk within $R_{\rm inner} < R_{\rm hole}$ (e.g., Lubow et al. 1999; Kley 1999; Bryden et al. 1999; D'Angelo et al. 2003; Bate et al. 2003; Lubow & D'Angelo 2006). While the *inner disk* ($r < R_{\rm inner} < R_{\rm hole}$) might then produce gaseous emission lines, the low surface filling factor of gas in the region of the gap would produce weak to

negligible emission because of the small projected emitting area of the accretion streams.

3. In the case of photoevaporation, gas in the region of the disk photoevaporation radius (few AU; Font et al. 2004; Liffman 2003) is being evaporated away faster than it can be replenished by viscous accretion. As a result, the inner disk is decoupled from the outer disk and accretes onto the star, leaving behind a true "inner hole" in the gas distribution and *no emission* from the region within $R_{\rm hole}$.

How do the properties of the gaseous inner disk of TW Hya compare with these predictions? UV fluorescent H_2 and CO fundamental emission, which are both believed to probe the inner ∼1 AU of T Tauri disks (see Najita et al. 2007a for a review), have been detected from the inner disk of TW Hya (Herczeg et al. 2002; Rettig et al. 2004; Salyk et al. 2007; Najita et al. 2007a). The spectroastrometric study of Pontoppidan et al. (2008) further demonstrates that the CO emission arises from a rotating disk close to the star (∼0.1 AU). Thus, the inner disk is not completely cleared of gas, a result that is consistent with the ongoing stellar accretion in the system and inconsistent with the EUV-driven photoevaporation scenario. (The situation is somewhat different if photoevaporation is driven by X-rays. Recent work by Ercolano and collaborators finds that photoevaporation driven by X-rays rather than EUV can create a transition-like SED at much higher disk masses and accretion rates than in the EUV-driven photoevaporation case. Under these conditions, the star may continue to accrete at a measurable rate for a longer fraction of the system lifetime after disk clearing has begun; Owen et al. 2010.)

The *Spitzer* spectrum allows us to probe the gaseous disk at radii beyond the region probed by UV fluorescent H_2 and CO fundamental emission, because the features in the SH spectrum probe emission from cooler gas. In the spectrum of AA Tau, a typical T Tauri star that possesses an optically thick inner disk, the molecular features detected in SH (H_2O, OH, C_2H_2, HCN, and CO_2), probe gas with temperatures of 300–600 K and disk emitting areas corresponding to a few AU in radius, i.e., the inner planet formation region of the disk (Carr & Najita 2008).

One of the most striking aspects of the *Spitzer* spectrum of TW Hya is the weak molecular emission compared to that seen in classical T Tauri stars such as AA Tau (Carr & Najita 2008; Salyk et al. 2008; J. S. Carr & J. R. Najita 2010, in preparation; K. M. Pontoppidan et al. 2010, in preparation). The scenario of a gap carved in the gaseous disk by an orbiting giant planet would appear to naturally lead to the suppression of the molecular emission from the inner disk region, like that observed. With the size of the optically thin region in the TW Hya system (∼4 AU) suggesting that an orbiting planet would reside at a few AU, we might expect the inner few AU region of the disk to be mostly cleared of gas.

In comparison, because it suggests a continuous gaseous disk with no continuum opacity in the inner region, the grain growth scenario might predict similar or stronger mid-infrared molecular emission than would be observed in a continuous disk of gas and dust such as AA Tau, as long as the molecular abundances of the inner disk are not significantly altered by the optically thin nature of the inner disk. Photodissociation may alter the molecular abundances in the disk, although molecular shielding (e.g., by CO, H_2, OH, and H_2O) may limit its impact. Another caveat is that molecules may be abundant in the inner disk of TW Hya, but molecular emission might not be excited to the level seen in AA Tau because of the lower accretion rate of TW Hya compared to typical T Tauri stars. A low accretion rate may imply a reduced rate of mechanical heating in the disk atmosphere. A low rate of mechanical heating can reduce the column density of warm water in the disk atmosphere (Glassgold et al. 2009) and lead to weak water emission.

There is observational motivation to consider these issues. Photodissocation by stellar UV photons may play a role in reducing molecular abundances in the disk, and the hot OH we see may provide evidence for the photodissociation of water in this system (Sections 3.5 and 4.2). The lack of grains in a gas-rich inner disk may also limit the molecular abundances in this region. Glassgold et al. (2009) have shown that processes such as the formation of H_2 on warm grain surfaces and mechanical heating associated with accretion can significantly enhance the abundance of water in the warm atmospheres of inner disks up to the levels observed in classical T Tauri disks. While it is yet unclear whether either of these is the dominant or critical factor in explaining the observed water abundances in classical T Tauri disk atmospheres, if H_2 formation on grains is an important requirement for the formation of H_2O in the warm disk atmosphere, the absence of grains in the inner disk region of a transition object may limit the H_2O emission from this region.

Thus, the lack of strong MIR molecular emission from TW Hya indicates that the inner planet formation region of its gaseous disk ($\lesssim$5 AU) has evolved away from the classical T Tauri norm. But further work is needed to determine whether that evolution is the result of the formation of a giant planet or other physical or chemical processes.

4.2. Origin of the Detected Emission

4.2.1. Molecular Emission

While strong molecular emission is not detected from TW Hya, we do detect a rich spectrum of weaker emission lines. Unlike the *Spitzer* spectrum of AA Tau (Carr & Najita 2008), which shows a rich spectrum of H_2O, OH, HCN, C_2H_2, and CO_2 emission, and the strong H_2O emission that is detected from the classical T Tauri stars DR Tau and AS 205A (Salyk et al. 2008), the molecular emission we detect from TW Hya in the 10–20 μm region is dominated by radicals (OH, and possibly CH_3) and ions (HCO^+).

Is the difference in the species detected in TW Hya versus classical T Tauri stars due to the physical truncation of the disk, as discussed in the previous section? Alternatively, or in addition, does the difference result from the higher X-ray and UV irradiation field of TW Hya? TW Hya has a nearly unique X-ray spectrum (Drake 2005) that shows unusually bright soft X-ray emission compared to other T Tauri stars (Robrade & Schmitt 2006). TW Hya is also known as a bright FUV emission source (Herczeg et al. 2004). Bergin et al. (2004) quote an FUV flux (including Lyα) of $G_0 = 3400$ at 100 AU for TW Hya, in comparison with values of 240, 340, and 1500 for DM Tau, GM Aur, and LkCa 15, respectively. One hypothesis is that the stronger UV and soft X-ray field of TW Hya results from its lower accretion rate ($10^{-9}\,M_\odot\,{\rm yr}^{-1}$; Muzerolle et al. 2000; Alencar & Basri 2000; Herczeg et al. 2004), which unburies the accretion shock and allows more energetic photons to emerge from the "sides" of the accretion column (Drake 2005; Ardila 2007; Ardila & Johns-Krull 2009).

Perhaps this higher intensity photon field is responsible for some aspects of the emission that we see. A stronger UV field from TW Hya may dissociate H_2O in favor of OH. The hot OH emission that we detect may provide evidence for this process

in action. This situation may therefore be similar to that of the Herbig Ae stars studied by Mandell et al. (2008), who suggested that the presence of OH emission and lack of H_2O emission from these sources could be the result of photodissociation by stellar UV.

If it arises from the photodissociation of water, the hot OH emission we observe may help to explain the origin of the high OH column density that is inferred for the disk atmospheres of classical T Tauri stars. Carr & Najita (2008) inferred a (line-of-sight) OH column density of 8×10^{16} cm^{-2} at a temperature of ~500 K based on their analysis of the *Spitzer* spectrum of AA Tau. For a system inclination of $i = 75$ for AA Tau (Bouvier et al. 2007), the measured OH column density corresponds to a vertical column density of 2×10^{16} cm^{-2}. Even larger OH column densities of 2×10^{17} cm^{-2} were inferred for two classical T Tauri stars based on 3 μm spectra (Salyk et al. 2008).

In comparison, Glassgold et al. (2009) find that X-ray irradiated disks will produce warm (300–1000 K) OH (vertical) column densities of 1×10^{14}–8×10^{14} cm^{-2}, with the specific value depending on the details of the model. Other chemical calculations for disks also fail to produce the large OH column densities (Agundez et al. 2008) or high OH/H_2O abundances (Woods & Willacy 2009) that are observed. Photodissociation of water to produce OH is one possible explanation for the much larger column density of OH that is observed (Bethell & Bergin 2009; Glassgold et al. 2009). The hot OH emission that we observe may provide observational support for that perspective.

When water in the disk absorbs dissociating UV photons, the UV photons can both produce hot (prompt) OH emission as well as heat the disk atmosphere. After it has emitted the prompt emission, the OH produced in this process may relax to a thermal distribution (at the gas temperature) and continue to emit thermally. A UV irradiated disk may thereby produce both thermal and prompt emission, as seen in a source such as AA Tau (Section 3.5). Detailed modeling is needed to determine if the OH emission observed in a system like AA Tau is consistent in detail with this picture.

Where would such water be located in the TW Hya system, given that no water emission is observed at 10–20 μm? One possibility is that it resides in the optically thin region of the disk, but it is not excited enough or warm enough to emit in the 10–20 μm region. Alternatively, the water may be present in the outer, optically thick disk where it is too cool to produce much emission at 10–20 μm. To address this issue, it would be interesting to measure velocity resolved OH line profiles in order to determine if the OH emission arises in a disk and at what radii.

The irradiation environment may also play a role in the HCO^+ emission that we detect. In their earlier study of organic molecules in the outer disk of TW Hya, Thi et al. (2004) found the abundance ratio of HCO^+/CO to be ~10 times larger in TW Hya than in two other transition disks (LkCa 15 and DM Tau). Thi et al. suggested that the high ratio of HCO^+/CO may result, in part, from the high X-ray flux of TW Hya. The high X-ray flux of TW Hya may also contribute to the prominence of HCO^+ emission in the mid-infrared.

4.2.2. Atomic Emission

As discussed in Section 3.4, the [Ne II] and [Ne III] fluxes we measure agree well with predictions for gaseous disks irradiated by stellar X-rays (see Section 3.4). EUV irradiation of the disk may also contribute to some extent, although a soft UV spectrum is needed to be consistent with the large [Ne II]/[Ne III] ratio observed. This result is consistent with the picture of a disk origin for the (spatially compact) [Ne II] emission from T Tauri stars that is probed by high-resolution spectroscopy. As discussed in Najita et al. (2009) based on high-resolution spectroscopy of [Ne II] emission from AA Tau and GM Aur, and Herczeg et al. (2007) in the context of TW Hya specifically, the [Ne II] emission line is symmetric, centered at the radial velocity of the star, and has line widths that are plausibly explained by disk rotation. The possibility of an origin in jets or outflows, illustrated in the case of the T Tau triplet (van Boekel et al. 2009), is less likely here, because TW Hya is not a known outflow source.

This perspective is basically confirmed, although with a twist, in the more recent study of [Ne II] in TW Hya using VISIR at the VLT. Pascucci & Sterzik (2009) interpret their measurement of the [Ne II] line profile of TW Hya, which shows a 6 km s^{-1} blueshift in the emission centroid, as indicating an origin in a low-velocity photoevaporative flow from the disk. This result is related to the idea of a disk origin for [Ne II] emission in that the emission still arises from disk gas, although it is gas that is gravitationally unbound rather than in hydrostatic equilibrium.

The H I emission we detect is not as well known or understood. While the 12.37 μm H I 7–6 line has been reported previously from T Tauri stars (e.g., Pascucci et al. 2007; see also Ratzka et al. 2007 for TW Hya), the weaker emission lines have not been reported previously. Perhaps such emission lines are commonly present in T Tauri stars, but they are obscured by stronger molecular emission and the weakness of the molecular emission in TW Hya makes the weaker H I lines easier to detect in this source. On the other hand, TW Hya is an energetic UV and X-ray emission source, as discussed above, and the emission we detect may be more unusual as a result.

What component of the T Tauri system could potentially produce the H I emission that we observe? Ratzka et al. (2007) suggested that the H I lines most likely originate from either an accretion shock or the stellar corona, although they were not specific on the details. Pascucci et al. (2007) have argued that the H I 6–5 and H I 7–6 emission detected from other low accretion rate T Tauri stars are too strong to be explained by magnetospheric accretion flows.

Following the lead of previous studies that interpreted the Brγ and Balmer lines of T Tauri stars as arising in a magnetospheric accretion flow (Calvet & Hartmann 1992; Hartmann et al. 1994; Najita et al. 1996; Muzerolle et al. 1998a, 1998b; Folha & Emerson 2001), Bary et al. (2008) interpreted the line ratios of the high-lying Paschen and Brackett lines they observed at low spectral resolution as arising in a magnetosphere with unusually low temperature. As described by Bary et al., the electron densities predicted theoretically for funnel flows (Martin 1996; Muzerolle et al. 2001) are consistent with their line ratios. They did not discuss whether magnetospheres can reproduce the fluxes of the Paschen and Brackett lines they observe.

The MIR H I lines impose further constraints on the origin of the H I emission. It is unclear whether the H I emission we observe can be produced by the accretion shocks that are discussed in the literature. The accretion shock in the TW Hya system is expected to have a height of ~ 1–1000 km for the post-shock region (Ardila & Johns-Krull 2009; Ardila 2007) and a density of ~10^{13} cm^{-3} (Drake 2005; Ardila 2007). The pre-shock region in typical T Tauri stars is characterized as having a temperature of ~ 10,000 K, a height of ~1000 km, an average density of 10^{11}–10^{15} cm^{-3}, and a filling factor of $f \sim 10^{-3}$–10^{-2} (Calvet & Gullbring 1998). These densities are

high enough to produce inverted H I populations (Hummer & Storey 1987). However, significant laser amplification may not occur or may be difficult to detect because of laser saturation and/or beaming effects (Strelnitski et al. 1996; Smith et al. 1997). Further work is needed to determine whether such high-density, compact regions can produce bright H I emission with roughly case B line ratios.

The line profiles of transitions connecting high-lying H I levels may also provide some insights. One example is the Paγ (6–3) profile of TW Hya (Edwards et al. 2006), which is superficially similar to a magnetospheric accretion profile: the profile is steeper on the red side than the blue and the blue wing extends to $\sim$300 km s^{-1}. However, as noted by Edwards et al., the profile is not consistent in detail with predictions for magnetospheric accretion, e.g., the profile is narrower and more centered than predicted profiles (e.g., Muzerolle et al. 2001). Such narrow Paγ profiles are found commonly for low accretion rate systems (Edwards et al. 2006).

Edwards et al. note a similarity with the narrow component of metallic emission lines (e.g., Fe I and Fe II), which are also the dominant component of the profile in low accretion sources such as TW Hya. The narrow and broad components are interpreted as arising in different physical regions, with the broad component having a significant contribution from funnel flows and an additional physically extended component from winds. The narrow component is associated with an accretion shock at the footpoint of the funnel flow (Edwards et al. 2006), which may not be the region from which the MIR H I emission originates, as noted above.

Disk atmospheres and/or photoevaporative flows may also contribute detectable H I emission. The disk atmosphere and photoevaporative flow that results from the X-ray irradiation of the disk, as described by Ercolano et al. (2008), produces a line luminosity of 4×10^{25} erg s^{-1} in the H I 7–6 (12.37 μm) line. In an updated calculation, Ercolano et al. (2009) solve for the hydrostatic structure of the disk and include irradiation by both EUV and X-rays. In this case, the H I 7–6 flux is revised upward to 4×10^{26} erg s^{-1} in FS0H0Lx1 (B. Ercolano 2009, private communication), a model that is fairly optimistic in assuming no attenuation of the EUV flux by foreground H I absorption (e.g., as might be present in a magnetosphere). We observe a yet larger luminosity of 1.8×10^{28} erg s^{-1}, the average of the flux in SH1 and SH2.

A more general question is whether the neon and H I emission can arise from the same physical region of the TW Hya system. The picture of [Ne II] and [Ne III] emission arising in a mostly neutral region (e.g., in an X-ray irradiated disk atmosphere; Section 3.4) contrasts, at least superficially, with the nominal picture of H I recombination line emission. Case B hydrogen line ratios are typically interpreted as indicating formation in a fully ionized region. (While a high ionization fraction is clearly not required to produce recombination emission, it helps to maximize the emission from a given mass of gas.)

The mismatch in these conditions seems to show up in other models of EUV and X-ray irradiated disks as well. Hollenbach & Gorti (2009) show that although irradiation by soft EUV can account for the flux of the [Ne II] emission observed from T Tauri stars, it cannot produce the observed H I 7–6 line luminosity: the predicted H I 7–6 flux is $<$ 1% of the [Ne II] flux. As a result, Hollenbach & Gorti (2009) argue that the H I emission arises from a different region than the [Ne II]. As they note, a high-density region is one possibility since it may produce significant H I emission without producing additional (unwanted) [Ne II]. Considerations of H I population inversions and laser amplification, and whether the H I emission would have (optically thin) case B line ratios, as described above, may limit the allowable range of densities.

Given the current uncertainty regarding the possible origin of the H I emission, it appears that high-resolution spectroscopy of the MIR H I lines would likely provide valuable, and much needed, insights into the origin of the emission. Since the 11.31 μm and 12.37 μm lines are comparable in brightness to the [Ne II] line, such a study should be feasible currently. If the mid-infrared lines are found to be as broad as the Paγ line, the role of high-velocity phenomena such as magnetospheric infall would be indicated. If the lines are narrow ($>$ 30 km s^{-1}) and/or with a small blueshift ($\sim$10 km s^{-1}), disk atmospheres and/or photoevaporative flows would be indicated.

Both components might in fact contribute. As noted above, the Paγ profiles of Edwards et al. (2006) are narrower and more centered in velocity than magnetospheric emission models. A combination of a high-velocity magnetospheric component and a low-velocity disk/photoevaporative component may better account for the observed profiles than a magnetosphere alone.

5. SUMMARY AND FUTURE DIRECTIONS

The *Spitzer* spectrum of TW Hya is strikingly different from that of other classical T Tauri stars reported in the literature, showing weak molecular emission in the 10–20 μm region and displaying no strong emission features of H_2O, C_2H_2, or HCN. Assuming that TW Hya was once a classical T Tauri star, the difference indicates that the inner planet formation region of its gaseous disk ($\lesssim$5 AU) has experienced significant evolution. With the SED of TW Hya indicating that the dust disk within $\sim$4 AU of the star has become optically thin in the continuum, possibly because it has been cleared by an orbiting giant planet (Calvet et al. 2002), it is tempting to infer that TW Hya shows weak molecular emission in the mid-infrared because the planet has created a gap in the *gaseous* disk as well. We discussed in Section 4 some of the issues that need to be investigated in order to determine whether the difference we observe is the result of giant planet formation or other processes.

Given our limited understanding of the factors that govern the emission spectra of T Tauri disks, it may be useful to take an empirical approach in exploring whether the lack of molecular emission seen from TW Hya is a consequence of the physical evolution of the disk, its chemical evolution, or an excitation effect. For example, to explore the possibility of an excitation effect, we can compare the *Spitzer* spectrum of TW Hya with those of other non-transition objects with comparable accretion rates. If non-transition objects with low accretion rates also lack strong molecular emission, the spectrum of TW Hya would not be unusual for its accretion rate and the lack of molecular emission may be the result of poor excitation. However, if strong molecular emission is observed in other low accretion rate systems, the absence of such emission in TW Hya would suggest a gap in its gaseous disk or a possible chemical effect. We will take this approach in a future study.

Similarly, it would be interesting to explore whether other transition objects also show weak molecular emission compared to classical T Tauri stars. If transition objects with much weaker UV fluxes than that of TW Hya (e.g., DM Tau, GM Aur) also show a deficit of molecular emission, that would suggest a more dominant role for SED evolution (a deficit of grains; possible clearing by a giant planet), rather than photochemistry,

in accounting for the difference in the spectra. We will report on this in future publications.

While strong molecular emission is not detected from TW Hya, we do detect a rich spectrum of emission lines of atoms (H I, [Ne II], and [Ne III]) and molecules (H_2, OH, CO_2, HCO^+, and possibly CH_3). One of the most intriguing is the OH emission, which is hot and may result from the UV photodissociation of water. A more detailed analysis of the OH emission spectrum may be able to determine whether it is produced by photodissociation. The properties of the molecular emission from TW Hya, both the OH and other molecules, will be analyzed in greater detail in a future study.

Because we detect multiple H I lines, we can show that the H I emission from TW Hya has a recombination spectrum. In contrast to the neon emission from TW Hya, which can be well accounted for by (primarily) stellar X-ray irradiation of the disk, the physical origin of the H I emission is difficult to identify. As discussed in Section 4, magnetospheres, disk atmospheres, and/or photoevaporative flows could plausibly contribute to the emission and multiple components may play a role. High-resolution spectroscopy of the brightest H I lines (H I 7–6 and H I 9–7) would likely provide valuable insights into the origin of the emission.

We are grateful to Al Glassgold, Barbara Ercolano, and David Ardila for interesting and useful discussions regarding the interpretation of the observations. J.N. thanks for their generous hospitality Tom Soifer and the Spitzer Science Center, where much of the analysis for this paper was carried out. This work is based on observations made with the *Spitzer Space Telescope*, which is operated by the Jet Propulsion Laboratory, California Institute of Technology under a contract with NASA. Support for this work was provided by NASA through an award issued by JPL/Caltech. Basic research in infrared astronomy at the Naval Research Laboratory is supported by 6.1 base funding.

Facility: Spitzer (IRS)

REFERENCES

Agundez, M., Cernicharo, J., Pardo, J. R., Guelin, M., & Philips, T. G. 2008, A&A, 485, L33
Alencar, S. H. P., & Basri, G. 2000, AJ, 119, 1881
Alencar, S. H. P., & Batalha, C. 2002, ApJ, 571, 378
Alexander, R. D., & Armitage, P. J. 2007, MNRAS, 375, 500
Alexander, R. D., & Armitage, P. J. 2009, ApJ, 704, 989
Alexander, R. D., Clarke, C. J., & Pringle, J. E. 2004, MNRAS, 348, 879
Alexander, R. D., Clarke, C. J., & Pringle, J. E. 2005, MNRAS, 358, 283
Alexander, R. D., Clarke, C. J., & Pringle, J. E. 2006, MNRAS, 369, 229
Ardila, D. R. 2007, in IAU Symp. 243, Star-Disk Interaction in Young Stars, ed. J. Bouvier & I. Appenzeller (Cambridge: Cambridge Univ. Press), 103
Ardila, D. R., & Johns-Krull, C. M. 2009, in AIP Conf. Proc. 1094, Proc. 15th Cambridge Workshop on Cool Stars, Stellar Systems and the Sun, Cool Stars, Stellar Systems and the Sun, ed. E. Stempels (Melville, NY: AIP), 309
Bary, J. S., Matt, S. P., Skrutskie, M. F., Wilson, J. C., Peterson, D. E., & Nelson, M. J. 2008, ApJ, 687, 376
Bate, M. R., Lubow, S. H., Ogilvie, G. I., & Miller, K. A. 2003, MNRAS, 341, 213
Bergin, E., et al. 2004, ApJ, 614, L133
Bethell, T., & Bergin, E. 2009, Science, 326, 1675
Bevington, P. R. 1969, Data Reduction and Error Analysis for the Physical Sciences (New York: McGraw-Hill), 235
Bezard, B., Romani, P. N., Feuchtgruber, H., & Encrenaz, T. 1999, ApJ, 515, 868
Bitner, M. A., et al. 2008, ApJ, 688, 1326
Bouvier, J., et al. 2007, A&A, 463, 1017
Bryden, G., Chen, X., Lin, D. N. C., Nelson, R. P., & Papaloizou, J. C. B. 1999, ApJ, 514, 344
Calvet, N., D'Alessio, P., Hartmann, L., Wilner, D., Walsh, A., & Sitko, M. 2002, ApJ, 568, 1008
Calvet, N., & Gullbring, E. 1998, ApJ, 509, 802
Calvet, N., & Hartmann, L. 1992, ApJ, 386, 239
Calvet, N., et al. 2005, ApJ, 630, L185
Carr, J. S., & Najita, J. R. 2008, Science, 319, 1504
Clarke, C. J., Gendrin, A., & Sotomayor, M. 2001, MNRAS, 328, 485
Cieza, L. A., Swift, J. J., Mathews, G. S., & Williams, J. P. 2008, ApJ, 686, L115
Coffey, D., Bacciotti, F., Woitas, J., Ray, T. P., & Eislöffel, J. 2004, ApJ, 604, 758
Davies, P. B., & Rothwell, W. J. 1984, J. Chem. Phys., 81, 5239
D'Angelo, G., Henning, T., & Kley, W. 2003, ApJ, 599, 548
Drake, J. J. 2005, in Proc. 13th Cambridge Workshop on Cool Stars, Stellar Systems and the Sun, ed. F. Favata, G. A. J. Hussain, & B. Battrick (ESA SP-560; Noordwijk: ESA), 519
Dullemond, C. P., & Dominik, C. 2005, A&A, 434, 971
Edwards, S., Fischer, W., Hillenbrand, L., & Kwan, J. 2006, ApJ, 646, 319
Ercolano, B., Clarke, C. J., & Drake, J. J. 2009, ApJ, 699, 1639
Ercolano, B., Drake, J. J., Raymond, J. C., & Clarke, C. J. 2008, ApJ, 688, 398
Espaillat, C., et al. 2007, ApJ, 664, L111
Feuchtgruber, H., Helmich, F. P., van Dishoeck, E. F., & Wright, C. M. 2000, ApJ, 535, L111
Flaccomio, E., Stelzer, B., Sciortino, S., Micela, G., Pillitteri, I., & Testi, L. 2009, A&A, 505, 695
Folha, D. F. M., & Emerson, J. P. 2001, A&A, 365, 90
Font, A. S., McCarthy, I. G., Johnstone, D., & Ballantyne, D. R. 2004, ApJ, 607, 890
Glassgold, A. E., Meijerink, R., & Najita, J. R. 2009, ApJ, 701, 142
Glassgold, A. E., Najita, J. R., & Igea, J. 2007, ApJ, 656, 515
Gorti, U., & Hollenbach, D. 2008, ApJ, 683, 287
Gorti, U., & Hollenbach, D. 2009, ApJ, 690, 1539
Guedel, M., et al. 2008, New Light on Young Stars: *Spitzer*'s View of Circumstellar Disks (Pasadena: CA: CalTech), http://www.ipac.caltech.edu/spitzer2008/talks/ManuelGuedel.html
Guedel, M., et al. 2009, A&A, submitted
Harich, S. A., et al. 2000, J. Chem. Phys., 113, 10073
Hartmann, L., Hewett, R., & Calvet, N. 1994, ApJ, 426, 669
Herczeg, G. J. 2007, in IAU Symp. 243, Star-Disk Interaction in Young Stars, ed. J. Bouvier & I. Appenzeller (Cambridge: Cambridge Univ. Press), 147
Herczeg, G. J., Linsky, J. L., Valenti, J. A., Johns-Krull, C. M., & Wood, B. E. 2002, ApJ, 572, 310
Herczeg, G. J., Najita, J. R., Hillenbrand, L. A., & Pascucci, I. 2007, ApJ, 670, 509
Herczeg, G. J., Wood, B. E., Linsky, J. L., Valenti, J. A., & Johns-Krull, C. M. 2004, ApJ, 607, 369
Hollenbach, D. J., & Gorti, U. 2009, ApJ, 703, 1203
Hollenbach, D. J., Yorke, H. W., & Johnstone, D. 2000, in Protostars and Planets IV, ed. V. Mannings, A. P. Boss, & S. S. Russell (Tucson, AZ: Univ. Arizona), 401
Houck, J. R., et al. 2004, Proc. SPIE, 5487, 62
Hughes, A. M., Wilner, D. J., Calvet, N., D'Alessio, P., Claussen, M. J., & Hogerheijde, M. R. 2007, ApJ, 664, 536
Hummer, D. G., & Storey, P. J. 1987, MNRAS, 224, 801
Johns-Krull, C. M., Valenti, J. A., & Linsky, J. L. 2000, ApJ, 539, 815
Kastner, J. H., Huenemoerder, D. P., Schulz, N. S., & Weintraub, D. A. 1999, ApJ, 525, 837
Kley, W. 1999, MNRAS, 303, 696
Lahuis, F., van Dishoeck, E. F., Blake, G. A., Evans, N. J., II, Kessler-Silacci, J. E., & Pontoppidan, K. M. 2007, ApJ, 665, 492
Lahuis, F., et al. 2006a, C2d Spectroscopy Explanatory Suppl. (Pasadena, CA: Spitzer Science Center)
Lahuis, F., et al. 2006b, ApJ, 636, 145
Lampton, M., Margon, B., & Bowyer, S. 1976, ApJ, 208, 177
Liffman, K. 2003, PASA, 20, 337
Lubow, S. H., & D'Angelo, G. 2006, ApJ, 641, 526
Lubow, S. H., Seibert, M., & Artymowicz, P. 1999, ApJ, 526, 1001
Mamajek, E. E. 2005, ApJ, 634, 1385
Mandell, A. M., Mumma, M. J., Blake, G. A., Bonev, B. P., Villanueva, G. L., & Salyk, C. 2008, ApJ, 681, L25
Marsh, K. A., & Mahoney, M. J. 1992, ApJ, 395, L115
Martin, S. C. 1996, ApJ, 470, 537
Meijerink, R., Glassgold, A. E., & Najita, J. R. 2008, ApJ, 676, 518
Muzerolle, J., Calvet, N., Briceño, C., Hartmann, L., & Hillenbrand, L. 2000, ApJ, 535, L47
Muzerolle, J., Calvet, N., & Hartmann, L. 1998a, ApJ, 492, 743
Muzerolle, J., Calvet, N., & Hartmann, L. 2001, ApJ, 550, 944
Muzerolle, J., Hartmann, L., & Calvet, N. 1998b, AJ, 116, 2965
Muzerolle, J., et al. 2009, ApJ, 704, L15

Najita, J., Carr, J. S., Glassgold, A. E., Shu, F. H., & Tokunaga, A. T. 1996, ApJ, 462, 919
Najita, J. R., Carr, J. S., Glassgold, A. E., & Valenti, J. A. 2007a, in Protostars and Planets V, ed. B. Reipurth, D. Jewitt, & K. Keil (Tucson, AZ: Univ. Arizona Press), 507
Najita, J. R., Crockett, N., & Carr, J. S. 2008, ApJ, 687, 1168
Najita, J. R., Strom, S. E., & Muzerolle, J. 2007b, MNRAS, 378, 369
Najita, J. R., et al. 2009, ApJ, 697, 957
Owen, J. E., Ercolano, B., Clarke, C. J., & Alexander, R. D. 2010, MNRAS, 401, 1415
Pascucci, I., & Sterzik, M. 2009, ApJ, 702, 724
Pascucci, I., et al. 2007, ApJ, 663, 383
Pascucci, I., et al. 2009, ApJ, 696, 143
Pontoppidan, K. M., Blake, G. A., van Dishoeck, E. F., Smette, A., Ireland, M. J., & Brown, J. 2008, ApJ, 684, 1323
Quillen, A. C., Blackman, E. G., Frank, A., & Varnière, P. 2004, ApJ, 612, L137
Ratzka, T., Leinert, C., Henning, T., Bouwman, J., Dullemond, C. P., & Jaffe, W. 2007, A&A, 471, 173
Rettig, T. W., Haywood, J., Simon, T., Brittain, S. D., & Gibb, E. 2004, ApJ, 616, L163
Rice, W. K. M., Wood, K., Armitage, P. J., Whitney, B. A., & Bjorkman, J. E. 2003, MNRAS, 342, 79
Robrade, J., & Schmitt, J. H. M. M. 2006, A&A, 449, 737
Salyk, C., Blake, G. A., Boogert, A. C. A., & Brown, J. M. 2007, ApJ, 655, L105
Salyk, C., Pontoppidan, K. M., Blake, G. A., Lahuis, F., van Dishoeck, E. F., & Evans, N. J., II. 2008, ApJ, 676, L49
Skrutskie, M. F., Dutkevitch, D., Strom, S. E., Edwards, S., Strom, K. M., & Shure, M. A. 1990, AJ, 99, 1187
Smith, H. A., Strelnitski, V., Miles, J. W., Kelly, D. M., & Lacy, J. H. 1997, AJ, 114, 2658
Stelzer, B., & Schmitt, J. H. M. M. 2004, A&A, 432, L35
Storey, P. J., & Hummer, D. G. 1995, MNRAS, 272, 41
Strelnitski, V. S., Ponomarev, V. O., & Smith, H. A. 1996, ApJ, 470, 1134
Strom, K. M., Strom, S. E., Edwards, S., Cabrit, S., & Skrutskie, M. F. 1989, AJ, 97, 1451
Tappe, A., Lada, C. J., Black, J. H., & Muench, A. A. 2008, ApJ, 680, L117
Thi, W.-F., van Zadelhoff, G.-J., & van Dishoeck, E. F. 2004, A&A, 425, 955
Uchida, K. I., et al. 2004, ApJS, 154, 439
van Boekel, R., Guedel, M., Henning, Th., Lahuis, F., & Pantin, E. 2009, A&A, 497, 137
Werner, M. W., et al. 2004, ApJS, 154, 1
Wilner, D. J., Ho, P. T. P., Kastner, J. H., & Rodríguez, L. F. 2000, ApJ, 534, L101
Woods, P. M., & Willacy, K. 2009, ApJ, 693, 1360